Transport Length Scales in Disordered Graphene-Based Materials: Strong Localization Regimes and Dimensionality Effects

Aurélien Lherbier,[1,3] Blanca Biel,[2] Yann-Michel Niquet,[3] and Stephan Roche[4,*]

[1]*Laboratoire des Technologies de la Microélectronique (LTM), UMR 5129 CNRS, CEA, 17 rue des Martyrs 38054 Grenoble, France*
[2]*LETI-MINATEC, CEA, 17 rue des Martyrs, 38054 Grenoble Cedex 9, France*
[3]*Institut des Nanosciences et Cryogénie, SP2M/L_sim, CEA, 17 avenue des Martyrs, 38054 Grenoble, France*
[4]*Institut des Nanosciences et Cryogénie, SPSMS/GT, CEA, 17 avenue des Martyrs, 38054 Grenoble, France*

(Received 30 August 2007; published 23 January 2008)

We report on a numerical study of quantum transport in disordered two dimensional graphene and graphene nanoribbons. By using the Kubo and the Landauer approaches, transport length scales in the diffusive (mean free path and charge mobilities) and localized regimes (localization lengths) are computed, assuming a short range disorder (Anderson-type). The electronic systems are found to undergo a conventional Anderson localization in the zero-temperature limit, in agreement with localization scaling theory. Localization lengths in weakly disordered ribbons are found to strongly fluctuate depending on their edge symmetry, but always remain several orders of magnitude smaller than those computed for 2D graphene for the same disorder strength. This pinpoints the role of transport dimensionality and edge effects.

DOI: 10.1103/PhysRevLett.100.036803 PACS numbers: 73.63.−b, 72.15.Rn, 81.05.Uw

Recently, a single graphene sheet could be isolated either from chemical exfoliation of bulk graphite [1], or by epitaxial growth on metal substrates through thermal decomposition of SiC [2]. These technological achievements have opened unprecedented opportunities to explore quantum transport in low dimensional carbon-based disordered systems [3,4].

Because of the unique electronic properties of the 2D graphene (massless Dirac fermions with linear dispersion and electron-hole symmetry), disorder effects and transport properties turn out to be unconventional. Theoretically, it has been shown that for long range impurity potentials, intervalley $K \rightarrow K'$ scattering between the two Dirac nodes could be strongly reduced, resulting in anomalously low backscattering rates [5], extremely large elastic mean free paths, and vanishingly small localization effects [6]. In contrast, for short range impurity potentials (where all types of scattering between K and K' are allowed), stronger quantum interferences could develop, leading to weak localization, or strong Anderson localization in the zero-temperature limit [7]. To date magnetotransport experiments performed either on exfoliated or epitaxial graphene have reported both weak antilocalization and weak localization effects [8], confirming the sensitivity of 2D transport in graphene to the external random potential, whose precise origin remains unknown.

Beyond 2D graphene physics, the transport properties of quasi-1D graphene nanoribbons (GNRs) with width down to a few tens of nanometers have been characterized [9]. In contrast to 2D graphene, the electronic properties of GNRs are strongly dependent on confinement effects and edge symmetries [10]. These new structures share similarities with carbon nanotubes, often viewed as rolled single graphene ribbons, and that have provided unique materials for investigating 1D transport phenomena such as Luttinger liquid and Kondo physics or Anderson localization [11].

The issue of localization in graphene-based materials is currently highly debated from a theoretical standpoint. For instance, the measurement of a minimal conductivity of ~ 2–$5e^2/h$ in samples for which charge mobilities change, however, by almost 1 order of magnitude remains to be fully understood [1–3]. Indeed, a conventional treatment of disorder effects within the self-consistent Born approximation (SCBA) yields $\sigma_{xx}^{\min} \sim 4e^2/(h\pi)$ for the two Dirac nodes [5] (h is the Planck constant), hence typically smaller by a $1/\pi$ factor with respect to the experimental data. Depending on the disorder model, the use of the Kubo approach suggests several scenarios to understand such discrepancies [12]. Besides, the role played by quantum interferences and the transition to a localization regime in graphene and GNRs remain poorly explored but fiercely debated [7].

In this Letter, by using both the Kubo and Landauer approaches, the transport length scales in 2D graphene are investigated and compared with those of the quasi-1D GNRs. The disorder (Anderson-type) is introduced via random fluctuations of the on-site energies of the π orbitals, which mimic a short range scattering potential that has been widely studied in the past as a generic disorder model in the framework of localization theory [13,14]. For 2D graphene, a real space order N Kubo method [15] is used to compute the energy-dependent elastic mean free path (ℓ_e), charge mobilities (μ), and semiclassical conductivities (σ_{sc}) in the diffusive regime, before quantum interferences come into play. Beyond the diffusive regime, the energy-dependent localization length (ξ) is extracted from the analysis of the transition from weak to strong localization, following the scaling theory phenomenology [14].

Quantum transport in GNRs with different chiralities (zigzag and armchair types) and the same disorder potential is also investigated within a Landauer approach [16]. For GNR widths in the range ~20–80 nm (within the experimental scope [9]), it is found that edge effects strongly enhance the impact of disorder, which results in localization lengths several orders of magnitude smaller than those obtained in 2D graphene for the same disorder strength.

The low energy electronic properties of 2D graphene are accurately described by the π-orbital tight-binding Hamiltonian, which is a first nearest neighbor two centers orthogonal p_z model, with on-site energies $\varepsilon_c = 0$ eV for all orbitals and the hopping term $\gamma_0 = 2.7$ eV. To mimic short range disorder, a white noise uncorrelated Anderson-type disorder is introduced as a random fluctuation of the on-site energies of the Hamiltonian ($\varepsilon = \varepsilon_c + \delta\varepsilon$). The scattering potential can thus be characterized by a single parameter W which defines the range of energy variations ($\delta\varepsilon \in [-W\gamma_0/2, +W\gamma_0/2]$), and thus allows us to tune the disorder strength. In what follows $W = [0.5, 2.5]$ enables the exploration of all transport regimes taking place in disordered 2D graphene and GNRs.

In Fig. 1, the density of states (DoS), computed with a Lanczos-type method [15], is reported as a function of W. The disorder-free DoS (dashed line) shows the typical behavior with a linear increase at low energy and the presence of two sharp van Hove singularities at $E = \pm\gamma_0$. As W is increased, two opposite behaviors are observed. At high energies, van Hove singularities are smoothened whereas close to the charge neutrality point (CNP), disorder enhances the DoS in agreement with prior analytical results [5] [see Fig. 1(b) for a close-up).

To investigate quantum transport in the 2D disordered graphene, an efficient real space and order N Kubo method is employed [15]. In this formalism, the mean free path $\ell_e(E)$, the semiclassical conductivity $\sigma_{sc}(E)$, and the charge carrier mobility $\mu(E)$ are deduced from the energy and time dependence of the diffusion coefficient $D(E, t) = \langle \Delta R^2 \rangle(E, t)/t$ (where $\langle \Delta R^2 \rangle(E, t)$ is the quadratic spread of random phase wave packets propagated in the graphene sheet).

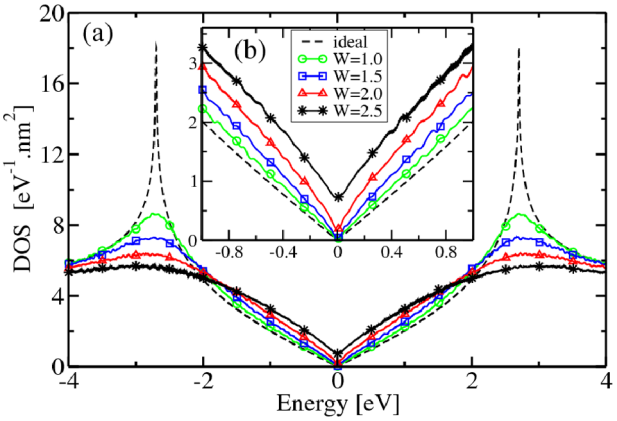

FIG. 1 (color online). (a) DoS of an ideal (dashed lines) and for disordered graphene sheets for several values of $W = 1, 1.5, 2, 2.5$. (b) Zoom in the energy area around the CNP.

In Fig. 2(c), the time dependence of $D(E, t)$ at the CNP and at $E = 0.1$ eV are reported for two values of W [17]. Different transport regimes follow each other as a function of the propagation time (or length). As expected, $D(E, t)$ first scales linearly with t at short times owing to the absence of elastic scattering. This linear scaling is followed by a saturation of D at a maximum value $D_{max}(E)$, which pinpoints the occurrence of a diffusive regime for which $D \sim v\ell_e$ (with v a group velocity and ℓ_e the elastic mean free path [15]). As evidenced in Fig. 2(c), the saturation time decreases with increasing disorder strength (W) or increasing charge energy (E). At longer times, $D(E, t)$ decreases owing to quantum interferences effects and localization phenomena [15]. The full energy dependence of ℓ_e is given in Fig. 2(b) for increasing W.

The strong enhancement of ℓ_e around the CNP results from the cusp in the DoS, which implies a reduced number of scattering processes. However, $\ell_e(E)$ drops from 180 nm at $W = 1.0$ to 10 nm at $W = 2.0$, as a consequence of the increase of the DoS close to CNP. In the weak disorder case ($W \in [0.2 - 0.7]$ not shown here), when the DoS at the CNP is almost unchanged with respect to the disorder-free graphene case, the behavior of $\ell_e(E)$ as a function of W is in good agreement with the Fermi golden rule (FGR); i.e., $\ell_e(E) \propto 1/W^2$. For higher values of W (1.0 to 2.0) slight deviations to the FGR are expected, since the weak disorder approximation is not strictly applicable anymore.

Figure 2(a) shows the corresponding charge mobilities deduced from $\mu(E) = \sigma_{sc}(E)/en(E)$, where $\sigma_{sc} = e^2\rho(E)v(E)\ell_e$ is the semiclassical conductivity deduced from the Einstein formula, $\rho(E)$ is the DoS, $n(E)$ is the charge density at energy E, and e is the elementary charge.

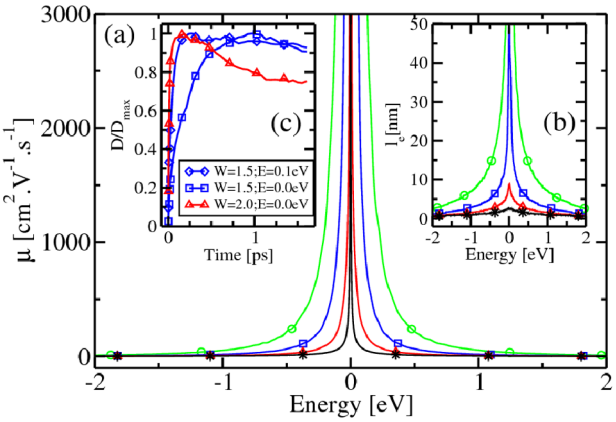

FIG. 2 (color online). Energy-dependent charge mobility (a) and mean free path (b) for the same values of W as in Fig. 1. (c) Diffusion coefficient $D(E, t)$ as a function of time for various disorder strengths and Fermi energies. $D(E, t)$ has been normalized with respect to its maximum value $D_{max}(E)$ to allow an easier comparison between the different curves.

The energy dependence of $\mu(E)$ and $\ell_e(E)$ is similar, and the sharp increase of $\mu(E)$ in the vicinity of CNP is in good qualitative agreement with some recent experimental results [2–4].

Experiments show that the conductivity (down to a few Kelvin) is almost constant close to the CNP, $\sigma(E=0) \sim 3$–$5e^2/h$, and weakly dependent on the value of the charge mobility [1–3]. On the theoretical side, within the SCBA the semiclassical part of the conductivity due to short range disorder is found to be $\sigma_{sc} = 4e^2/(h\pi)$ [5]. By using the Kubo formalism, it was further found that $\sigma(E=0)$ strongly depends on the nature of the scattering potential (short or long range) [12]. Our numerical results are shown in Fig. 3(b). σ_{sc} clearly remains larger or equal to $\sigma_{min} = 2G_0/\pi$ ($G_0 = 2e^2/h$), a fact that would be consistent with the Mott argument [14], although localization effects are further observed at all energies (see hereafter). Besides, the shape of the energy dependence of conductivity is in perfect agreement with prior analytical results derived for short range disorder within the SCBA [5].

However, the conductivity would not be sensitive to localization effects only in the presence of some decoherence mechanisms such as electron-electron scattering of electron-phonon coupling [14]. In contrast, as previously seen in the time dependence of the diffusion coefficient [Fig. 2(c)], our zero-temperature calculations evidence the contribution of localization effects that develop beyond the diffusive regime. The 2D localization length ξ can be evaluated as follows [14]: Whatever the disorder model, the quantum correction to the conductivity is expected to scale as $\Delta\sigma(L) = (G_0/\pi)\ln(L/\ell_e)$, where L is the length scale associated with the propagation time. The localization length ξ is given by $\Delta\sigma(L=\xi) = \sigma_{sc}$; i.e., $\xi = \ell_e \exp(\pi\sigma_{sc}/G_0)$. Our results are reported in Fig. 3(a) for several disorder strengths (averages over several tens of configurations has been performed). The energy dependence of ξ is mainly dominated by that of σ_{sc}. As a result,

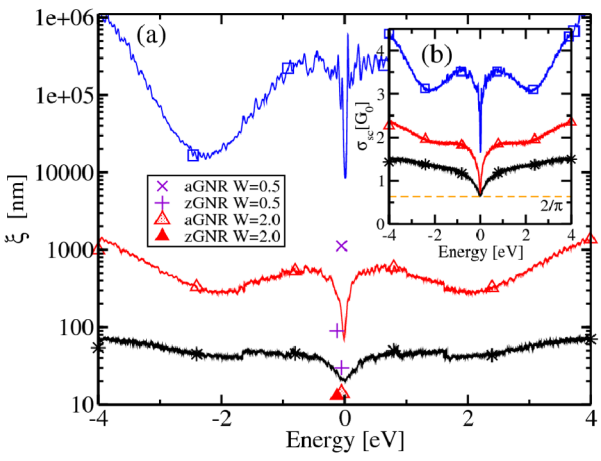

FIG. 3 (color online). (a) $\xi(E)$ for three disorder strengths (same legend as in Fig. 1). (b) Energy-dependent semiclassical conductivity for the same disorder strengths.

although ℓ_e is strongly increasing as the Fermi level moves toward the CNP (undoped case), the behavior of ξ shows an opposite trend, with a minimum value at CNP.

Recently, the possibility to fabricate quasi-1D graphene nanoribbons has opened new perspectives for future carbon-based nanoelectronics [2,9]. It is thus important to evaluate the effects of disorder in this situation of lower transport dimensionality.

The band structures of ideal GNRs with width below $\sim$100 nm and well defined edge symmetries (zigzag or armchair types) are dominated by confinement effects and van Hove singularities [10], similarly to carbon nanotubes [11]. As for the case of 2D graphene, we have used the nearest neighbor tight-binding approximation, which has been widely employed for studying transport properties in pure or defected GNRs [10,18]. More sophisticated tight-binding models (next nearest neighbor tight-binding [19]) or *ab initio* calculations [20] bring some modifications of band structure at energies close to the CNP. However, our calculations will be performed at energies sufficiently far away from the CNP to preserve the generality of our results.

Zigzag-type GNRs (zGNRs) show very peculiar electronic properties with wave functions sharply localized along the GNR edges at low energies. By using a Landauer approach [16,18,21], the conductance for both types of symmetries is computed for the ideal case [Fig. 4(a)] and for a single disorder configuration, with varying disorder strength [Figs. 4(b) and 4(d)]. For weak disorder [$W = 0.5$, Fig. 4(b)], it clearly appears that armchair GNR (aGNR) is less sensitive to disorder effects than zigzag GNR. In Figs. 4(c) and 4(e), the averaged normalized conductances are shown to follow an exponential scaling behavior, allowing to extract localization lengths from $\langle \ln G/G_0 \rangle \sim L/\xi$ (averaged over $\sim$400 configurations). The extracted $\xi(E)$ at selected energies [see the arrows in Fig. 4(a)] are further reported in Fig. 3 (as single cross or triangle). For disorder as large as $W = 2$ [Fig. 4(d)], the localization lengths are similar for both types of ribbons, showing that edge symmetry does not play any role. In contrast, ξ is up to 2 orders of magnitude smaller in zigzag than in armchair GNRs in the low disorder limit ($W = 0.5$), choosing an energy far from the close vicinity of the CNP (following [18]). This result can be understood by the lower transport dimensionality in the case of zigzag edge symmetry, driven by more confined wave functions [10]. However, ξ remains always several orders of magnitude smaller in GNRs than in 2D graphene, whatever the disorder strength (see Fig. 3). Similar results are obtained for GNRs with a larger width of $\simeq$ 80 nm (not shown).

In conclusion, by studying the transport properties in both disordered 2D graphene and GNRs (for short range scattering potential), the impact of dimensionality on transport length scales was investigated. Despite the simplicity

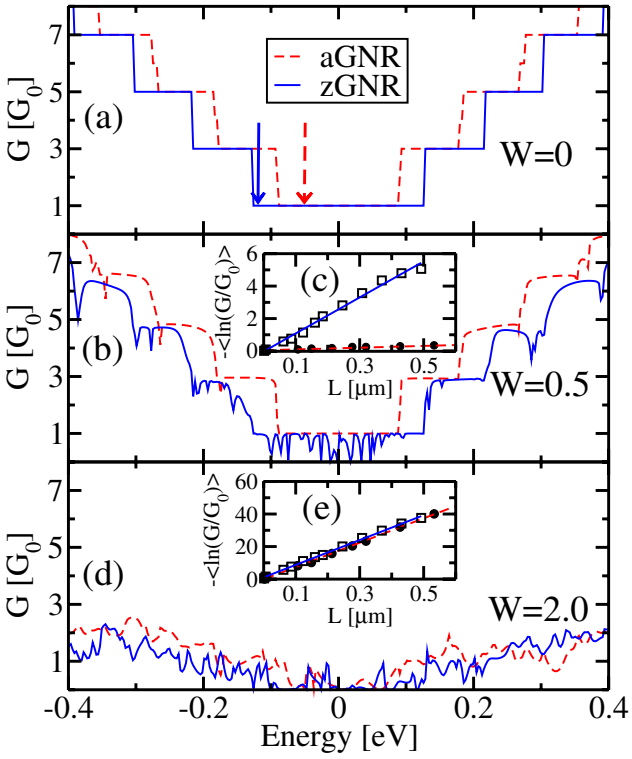

FIG. 4 (color online). (a) Conductance for ideal zigzag [solid (blue) line] and armchair [dashed (red) line] GNRs with a width of ~20 nm. (b) Conductance for a single disorder configuration of a zigzag [solid (blue) line] and an armchair [dashed (red) line] GNR with width ~20 nm and for $W = 0.5$. (c) Configuration averaged (over ~400 samples) normalized conductance as a function of GNR length for both zigzag and armchair GNRs. The solid (blue) [dashed (red)] arrows in (a) show the energy at which the calculations for the zGNR [aGNR] have been performed. (d),(e) Same information as for (b) and (c) but for a larger disorder strength ($W = 2$).

of the Anderson model, some of the reported transport features may be generic to other types of disorder such as chemical doping, surface functionalization, or topological defects. However, the contribution of long range potentials (e.g., due to ionized impurities [12]) deserves further consideration.

B. B. acknowledges the CARNOT Institute-LETI for financial support. We thank the CEA/CCRT supercomputing facilities for providing computational resources.

*Corresponding author.
stephan.roche@cea.fr

[1] K. S. Novoselov *et al.*, Science **306**, 666 (2004); K. S. Novoselov *et al.*, Nature (London) **438**, 197 (2005); A. K. Geim and K. S. Novoselov, Nat. Mater. **6**, 183 (2007).
[2] C. Berger *et al.*, Science **312**, 1191 (2006).
[3] M. I. Katsnelson, K. S. Novoselov, and A. K. Geim, Nature Phys. **2**, 620 (2006); K. S. Novoselov *et al.*, Nature Phys. **2**, 177 (2006); K. S. Novoselov *et al.*, Science **315**, 1379 (2007); Y. Zhang, Y.-W. Tan, H. L. Stormer, and Ph. Kim, Nature (London) **438**, 201 (2005).
[4] Y. W. Tan *et al.*, Phys. Rev. Lett. **99**, 246803 (2007).
[5] N. H. Shon and T. Ando, J. Phys. Soc. Jpn. **67**, 2421 (1998); Y. Zheng and T. Ando, Phys. Rev. B **65**, 245420 (2002).
[6] E. McCann *et al.*, Phys. Rev. Lett. **97**, 146805 (2006); P. M. Ostrovsky, I. V. Gornyi, and A. D. Mirlin, Phys. Rev. B **74**, 235443 (2006); A. F. Morpurgo and F. Guinea, Phys. Rev. Lett. **97**, 196804 (2006); D. V. Khveshchenko, Phys. Rev. B **75**, 241406 (2007); K. Wakabayashi, Y. Takane, and M. Sigrist, Phys. Rev. Lett. **99**, 036601 (2007).
[7] V. I. Fal'ko *et al.*, Solid State Commun. **143**, 33 (2007); H. Suzuura and T. Ando, J. Phys. Soc. Jpn. **75**, 024703 (2006); A. Altland, Phys. Rev. Lett. **97**, 236802 (2006); I. L. Aleiner and K. B. Efetov, Phys. Rev. Lett. **97**, 236801 (2006); K. Nomura, M. Koshino, and S. Ryu, Phys. Rev. Lett. **99**, 146806 (2007).
[8] S. V. Morozov *et al.*, Phys. Rev. Lett. **97**, 016801 (2006); X. Wu *et al.*, Phys. Rev. Lett. **98**, 136801 (2007).
[9] M. Y. Han *et al.*, Phys. Rev. Lett. **98**, 206805 (2007); M. C. Lemme *et al.*, IEEE Electron Device Lett. **28**, No. 4, 282 (2007).Z. Chen *et al.*, Physica (Amsterdam) **40E**, 228 (2007).
[10] K. Nakada *et al.*, Phys. Rev. B **54**, 17 954 (1996); K. Wakabayashi *et al.*, Phys. Rev. B **59**, 8271 (1999); N. Peres, A. H. Castro Neto, and F. Guinea, Phys. Rev. B **73**, 195411 (2006); F. Muñoz-Rojas *et al.*, Phys. Rev. B **74**, 195417 (2006).
[11] J. C. Charlier, X. Blase, and S. Roche, Rev. Mod. Phys. **79**, 677 (2007).
[12] K. Ziegler, Phys. Rev. Lett. **97**, 266802 (2006); Phys. Rev. B **75**, 233407 (2007); K. Nomura and A. H. MacDonald, Phys. Rev. Lett. **96**, 256602 (2006); **98**, 076602 (2007); E. H. Hwang, S. Adam, and S. Das Sarma, Phys. Rev. Lett. **98**, 186806 (2007); J. Cserti, Phys. Rev. B **75**, 033405 (2007).
[13] P. W. Anderson, Phys. Rev. **124**, 41 (1961); E. Abraham *et al.*, Phys. Rev. Lett. **42**, 673 (1979).
[14] P. A. Lee and D. S. Fisher, Phys. Rev. Lett. **47**, 882 (1981); P. A. Lee and T. V. Ramakrishnan, Rev. Mod. Phys. **57**, 287 (1985).
[15] F. Triozon *et al.*, Phys. Rev. B **69**, 121410 (2004).
[16] S. Datta, *Electronic Transport in Mesoscopic Systems* (Cambridge University Press, Cambridge, 1995).
[17] Periodic boundary conditions are used. Convergence is achieved for typical supercell sizes $L_x = 320$ nm and $L_y = 185$ nm, enclosing more than 2×10^6 carbon atoms.
[18] D. A. Areshkin, D. Gunlycke, and C. T. White, Nano Lett. **7**, 204 (2007); D. Gunlycke, D. A. Areshkin, and C. T. White, Appl. Phys. Lett. **90**, 142104 (2007); D. Gunlycke, H. M. Lawler, and C. T. White, Phys. Rev. B **75**, 085418 (2007).
[19] K. Sasaki, S. Murakami, and R. Saito, Appl. Phys. Lett. **88**, 113110 (2006).
[20] Y.-W. Son, M. L. Cohen, and S. G. Louie, Nature (London) **444**, 347 (2006).
[21] B. Biel *et al.*, Phys. Rev. Lett. **95**, 266801 (2005); R. Avriller *et al.*, Phys. Rev. B **74**, 121406 (2006).